International Journal of Solids and Structures 46 (2009) 2739–2749

Contents lists available at ScienceDirect

International Journal of Solids and Structures

journal homepage: www.elsevier.com/locate/ijsolstr

Cohesive zone modeling of interfacial delamination in PZT thin films

Yabin Yan, Fulin Shang *

MOE Key Laboratory for Strength and Vibration, Department of Engineering Mechanics, School of Aerospace, Xi'an Jiaotong University, 28 West, Xianning Road, Xi'an 710049, China

ARTICLE INFO

Article history:
Received 12 November 2008
Received in revised form 5 March 2009
Available online 18 March 2009

Keywords:
Thin film
Interface
Delamination
Cohesive zone model

ABSTRACT

Previous experimental investigations [Shang, F., Kitamura, T., Hirakata, H., Kanno, I., Kotera, H., Terada, K., 2005. Experimental and theoretical investigations of delamination at free edge of interface between piezoelectric thin films on a substrate. International Journal of Solids and Structures 42 (5–6) 1729–1741] have demonstrated that multilayered Cr/PZT/PLT/Pt/Ti thin films deposited on single-crystal silicon substrates are delaminated along the interface between Cr and PZT layers in a brittle manner. This study starts with a model based on the cohesive zone concept and carries out numerical simulations to check the fracture behavior of this interfacial delamination. Three types of cohesive zone models (CZMs) are adopted, including the exponential, bilinear, and trapezoidal models. Characteristic CZM parameters are extracted through comparisons with experimental results. The simulation results show that (i) cohesive strength and work of separation are the dominating parameters in the CZMs; (ii) the bilinear CZM more suitably describes this brittle interfacial delamination; and (iii) in comparison with typical several mm-thick film/coating materials, the fracture energy of this weak Cr/PZT interface is quite low. Our study demonstrates the applicability of CZM in characterizing the interface fracture behavior of film materials with micrometer thicknesses.

1. Introduction

Many functional devices using piezoelectric thin films are made from multi-layered thin films of different materials with many interfaces; however, these bi-material interfaces frequently delaminate during processing. Delamination occurs especially at the free edge of thin films because of stress concentration due to the mismatch of deformation, leading to failure of these devices (Evans and Hutchinson, 1995; Kong and En, 2006). Therefore, it is very important to evaluate the interface strength between thin film layers on a substrate.

In previous experimental tests (Shang et al., 2005), $Pb(Zr_{0.53}, Ti_{0.47})O_3$ (PZT) thin films were deposited by sputtering different metal or ceramic layers onto a single-crystal silicon substrate. A final sequence of six film layers, Cr/PZT/PLT/Pt/Ti/Si, was obtained for all of the tested specimens. A series of sandwiched-cantilever-type specimens were tested in the experimental setup schematically depicted in Fig. 1. The load, P, was applied over the left edge of the cantilever using a SHIMAZU micro-material testing system, MCTE-500. The experimental results show that: (1) the obtained load–displacement curves of the specimens are almost linear up to delamination, as shown in Fig. 2; (2) delamination initiates at the free edge of the interface between the Cr layer and PZT layer and propagates along the interface; and (3) fracture takes place abruptly after crack initiation, and the interface fails in a brittle manner with no noticeable plasticity.

The experimental results only provide the fracture loads of these specimens, which cannot be used to characterize the interfacial toughness of the thin films. Furthermore, the external work does not represent the interfacial fracture energy because the total work due to the external load is not only transformed into strain energy that is stored in the specimens, but is also expended in overcoming the resistance of crack initiation and propagation along the interface. Therefore, an unresolved issue is deciding which parameter should be used to evaluate the interfacial toughness of the thin films. This study aims to establish an appropriate mechanical model to simulate the interfacial delamination occurring in the previous experiments and extract the characteristic parameter that represents the interfacial toughness of the Cr/PZT/PLT/Pt/Ti thin films.

There exist two points of view as to how to characterize and evaluate the mechanical properties associated with interfacial bonding in thin films (Yang et al., 2007). From the point of view of stress, parameters such as interface bonding strengths (including tensile strength and shear strength), critical stress intensity factor, and energy release rate are widely used in the literature. The alternative point of view is based on the energy concept (Volinsky et al., 2002). This usually provides two parameters, viz., interfacial toughness or interfacial fracture toughness, representing, respectively, the energy per unit area consumed during the entire process, from the initial deformation to the final fracture of

* Corresponding author. Tel.: +86 29 82668757 803; fax: +86 29 82660977.
E-mail address: shangfl@mail.xjtu.edu.cn (F. Shang).

0020-7683/$ - see front matter © 2009 Elsevier Ltd. All rights reserved.
doi:10.1016/j.ijsolstr.2009.03.002

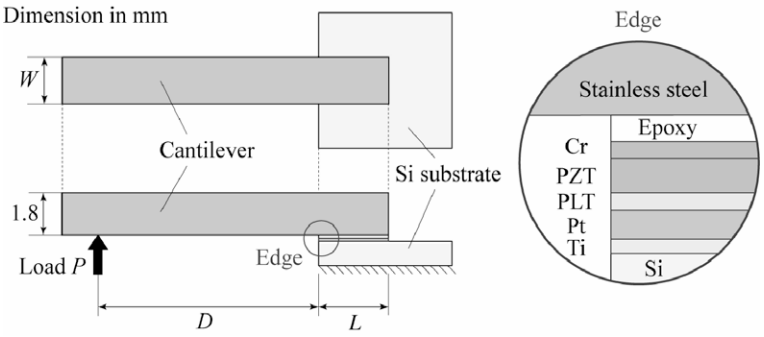

Fig. 1. Schematics of the sandwiched cantilever specimen and loading system.

interfaces, or the resistance to crack propagation for an interface with a pre-crack. For interfaces having simple geometries and specific bi-material combinations, the approach based on stress or stress intensity factor was proven to be rather effective and also convenient to implement (Akisanya and Meng, 2003); however, this type of approach has some deficiencies. First, the stress intensity parameters for delamination crack initiation of interface edges depend on specimen geometry. Therefore, the derived interfacial toughness parameter is also related to the specimen geometry. Second, the stress intensity parameter as the crack initiation toughness is different with the governing parameter of crack propagation along the interface both in dimensions and value, because the stress singularity order varies immediately after crack initiation (e.g., Akisanya and Meng, 2003; Shang et al., 2005). Third, previous studies have shown that increasingly thinner films exhibit increasingly smaller stress intensity dominance zones (Becker et al., 1997). In view of these deficiencies, the method based on the energy concept is more appropriate because it can at least be used to describe both crack initiation and crack propagation. The parameter that represents the interfacial bonding strength only depends on the intrinsic properties of the thin films, and does not depend on specimen geometry. The CZM in continuum mechanics is one of such methods. The CZM has been widely used to describe fracture and failure in metals, ceramics, polymers, and composite materials, and has successfully interpreted a variety of problems, such as crack tip plasticity and creep, crazing in polymers, and adhesively bonded joints and interface cracking in bi-materials (Wei and Hutchinson, 1997; Mohammed and Liechti, 2000; Chandra et al., 2002; Feraren and Jensen, 2004; Xu and Needleman, 1993; Geubelle and Baylor, 1998).

In this work, three different types of CZMs, including bilinear, exponential, and trapezoidal, will be used to simulate the interface delamination of the multilayered Cr/PZT/PLT/Pt/Ti thin films on a silicon substrate discussed in the aforementioned experimental tests. The bonding strength of the Cr/PZT interface will be extracted and then discussed in detail.

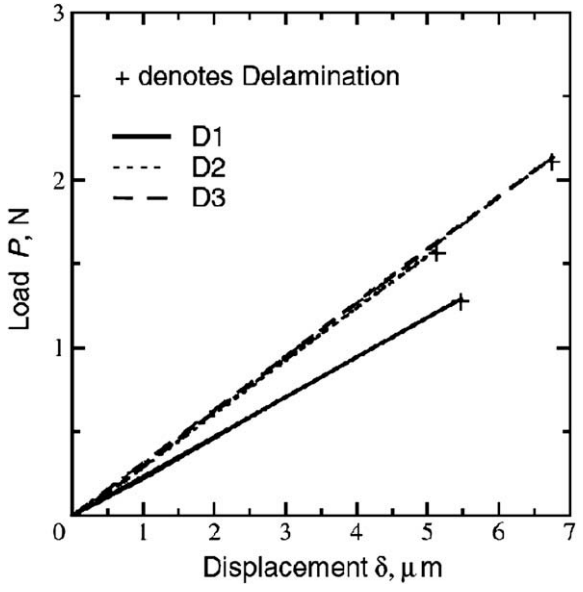

Fig. 2. Load–displacement curves of the sandwiched cantilever specimens.

2. Cohesive zone model

The cohesive zone model was originally used to describe the interaction between atoms or molecules. In the current literature, CZM is commonly regarded as a phenomenological model within a continuum mechanics framework. Historically, Barenblatt (1962) was one of the pioneers who developed CZMs to investigate the fracture behavior of perfectly brittle materials, in which the cohesive traction acting across the gap between two adjacent planes of dissimilar elastic materials represents atomic interaction. For cracks in a solid, a small atomic cohesive force zone was supposed to exist at the vicinity of the crack tip. Dugdale (1960) extended this concept to perfectly plastic materials by postulating the existence of a process zone at the crack tip. Within this zone, a simplified model for fracture problems was proposed by adopting a constitutive relation between cohesive traction and separation, otherwise known as the so-called cohesive law. Its essential features are the work per unit area required for separation of surfaces and the maximum cohesive traction that arises in the process (cohesive strength). The work of separation is the characteristic parameter of the interface, independent of specimen dimensions. The necessary driving force to effect interface delamination must overcome the work of separation plus the work of plastic deformation per unit area. Needleman (1987, 1990) used polynomial and exponential types of cohesive laws to simulate particle debonding in metal matrices. Xu and Needleman (1993, 1994) adopted these models to study void nucleation at the interface between the particle and matrix, and the dynamic fracture growth at the bi-material interfaces. Tvergaard and Hutchinson (1992) proposed a trapezoidal type of CZM to determine crack growth resistance. Camacho and Ortiz (1996) utilized a linear type of CZM to simulate multiple cracking along arbitrary paths under impact damage in brittle materials. Geubelle and Baylor (1998) employed a bilinear CZM to simulate the crack initiation and propagation of transverse matrix cracks and delamination in a thin composite plate due to low-velocity impacts. The traction–separation relations for most of the CZMs are such that, with the increase of the interfacial separation, the traction across the interface initially increases and

reaches a maximum, and then decreases and finally vanishes permitting a complete decohesion. These CZMs differ in the shape and the factors that describe the shape.

In this study, bilinear, exponential, and trapezoidal CZMs will be used to simulate the interfacial delamination of the PZT thin films occurring in the aforementioned sandwiched cantilever tests. These three CZMs are briefly introduced here.

2.1. Exponential CZM

For the exponential CZM, an interfacial potential is defined by

$$\phi(\Delta_n,\Delta_t)=\phi_n+\phi_n\exp\left(-\frac{\Delta_n}{\delta_n}\right)\left\{\left[1-r+\frac{\Delta_n}{\delta_n}\right]\frac{1-q}{r-1}-\left[q+\left(\frac{r-q}{r-1}\right)\frac{\Delta_n}{\delta_n}\right]\exp\left(-\frac{\Delta_t^2}{\delta_t^2}\right)\right\} \quad (1)$$

where $q=\phi_t/\phi_n$, $r=\Delta_n^*/\delta_n$; ϕ_n and ϕ_t are the works of the normal and tangential separations, respectively; Δ_n and Δ_t are the normal and tangential displacement jumps, respectively; δ_n and δ_t are the normal and tangential interface characteristic length parameters; Δ_n^* is the value of Δ_n after complete shear separation occurs under the condition of vanishing normal traction.

The relations between the traction across an interface and the potential are

$$T_n=\frac{\partial\phi}{\partial\Delta_n},\qquad T_t=\frac{\partial\phi}{\partial\Delta_t} \quad (2)$$

Substituting Eq. (1) into Eq. (2) gives the interfacial tractions as follows:

$$T_n=-\left(\frac{\phi_n}{\delta_n}\right)\exp\left(-\frac{\Delta_n}{\delta_n}\right)\left\{\frac{\Delta_n}{\delta_n}\exp\left(-\frac{\Delta_t^2}{\delta_t^2}\right)+\frac{1-q}{r-1}\left[1-\exp\left(-\frac{\Delta_t^2}{\delta_t^2}\right)\right]\left(r-\frac{\Delta_n}{\delta_n}\right)\right\} \quad (3)$$

$$T_t=-\frac{\phi_n}{\delta_n}\left(\frac{2\delta_n}{\delta_t}\right)\frac{\Delta_t}{\delta_t}\left(q+\frac{r-q}{r-1}\frac{\Delta_n}{\delta_n}\right)\exp\left(-\frac{\Delta_n}{\delta_n}\right)\exp\left(-\frac{\Delta_t^2}{\delta_t^2}\right) \quad (4)$$

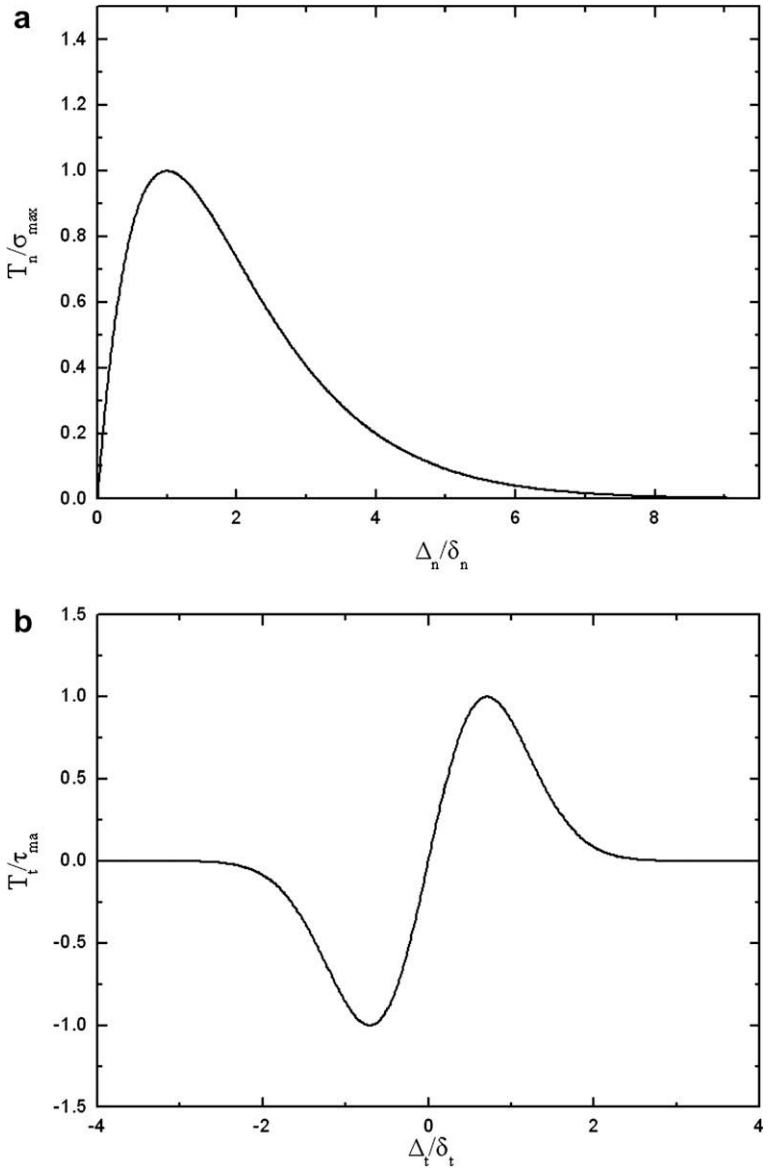

Fig. 3. (a) Normal and (b) tangential traction–separation curves for the exponential CZM.

The works of normal and shear separations are related to the peak normal traction, σ_{max}, and the peak tangential traction, τ_{max}, respectively,

$$\phi_n = \sigma_{max}\delta_n \exp(1), \qquad \phi_t = \sqrt{\exp(1)/2}\tau_{max}\delta_t \tag{5}$$

With $\Delta_t = 0$, the normal traction–separation relation given by Eq. (3) is shown in Fig. 3(a), while Fig. 3(b) shows the tangential traction–separation relation subject to $\Delta_n = 0$.

2.2. Bilinear CZM

The interfacial constitutive relations for the bilinear CZM are given by the following:

For $\widetilde{\Delta}_n > 0$,

$$T_n = \begin{cases} \frac{\widetilde{\Delta}_n}{\Delta_{max}}\sigma_{max}, & (\widetilde{\Delta} \leqslant \widetilde{\Delta}_{max}) \\ \frac{\widetilde{\Delta}_n}{\widetilde{\Delta}}\frac{1-\widetilde{\Delta}}{1-\Delta_{max}}\sigma_{max}, & (\widetilde{\Delta} > \widetilde{\Delta}_{max}) \end{cases} \tag{6}$$

$$T_t = \begin{cases} \frac{\widetilde{\Delta}_t}{\Delta_{max}}\frac{\Delta_n^c}{\Delta_t^c}\sigma_{max}, & (\widetilde{\Delta} \leqslant \widetilde{\Delta}_{max}) \\ \frac{\widetilde{\Delta}_t}{\widetilde{\Delta}}\frac{1-\widetilde{\Delta}}{1-\Delta_{max}}\frac{\Delta_n^c}{\Delta_t^c}\sigma_{max}, & (\widetilde{\Delta} > \widetilde{\Delta}_{max}) \end{cases} \tag{7}$$

For $\widetilde{\Delta}_n = 0$,

$$T_t = \begin{cases} \frac{\widetilde{\Delta}_t}{\Delta_{max}}\frac{\Delta_n^c}{\Delta_t^c}\sigma_{max}, & (\widetilde{\Delta} \leqslant \widetilde{\Delta}_{max}) \\ \frac{\widetilde{\Delta}_t}{\widetilde{\Delta}}\frac{1-\delta}{1-\delta_{max}}\frac{\Delta_n^c}{\Delta_t^c}\sigma_{max}, & (\widetilde{\Delta} > \widetilde{\Delta}_{max}) \end{cases} \tag{8}$$

where σ_{max} and τ_{max} are the interface normal strength and tangential strength, respectively; Δ_n^c and Δ_t^c are the critical normal and tangential separations when complete separation occurs; $\widetilde{\Delta}_n$, $\widetilde{\Delta}_t$, and $\widetilde{\Delta}$ are the non-dimensional normal, tangential, and total displacement jumps, respectively, and defined as

$$\widetilde{\Delta}_n = \frac{\Delta_n}{\Delta_n^c}, \quad \widetilde{\Delta}_t = \frac{\Delta_t}{\Delta_t^c}, \quad \widetilde{\Delta} = \sqrt{\widetilde{\Delta}_n^2 + \widetilde{\Delta}_t^2} \tag{9}$$

$\widetilde{\Delta}_{max}$ is the corresponding value of $\widetilde{\Delta}_n$ or $\widetilde{\Delta}_t$ when the interface normal strength or tangential strength reaches its peak value (Fig. 7).

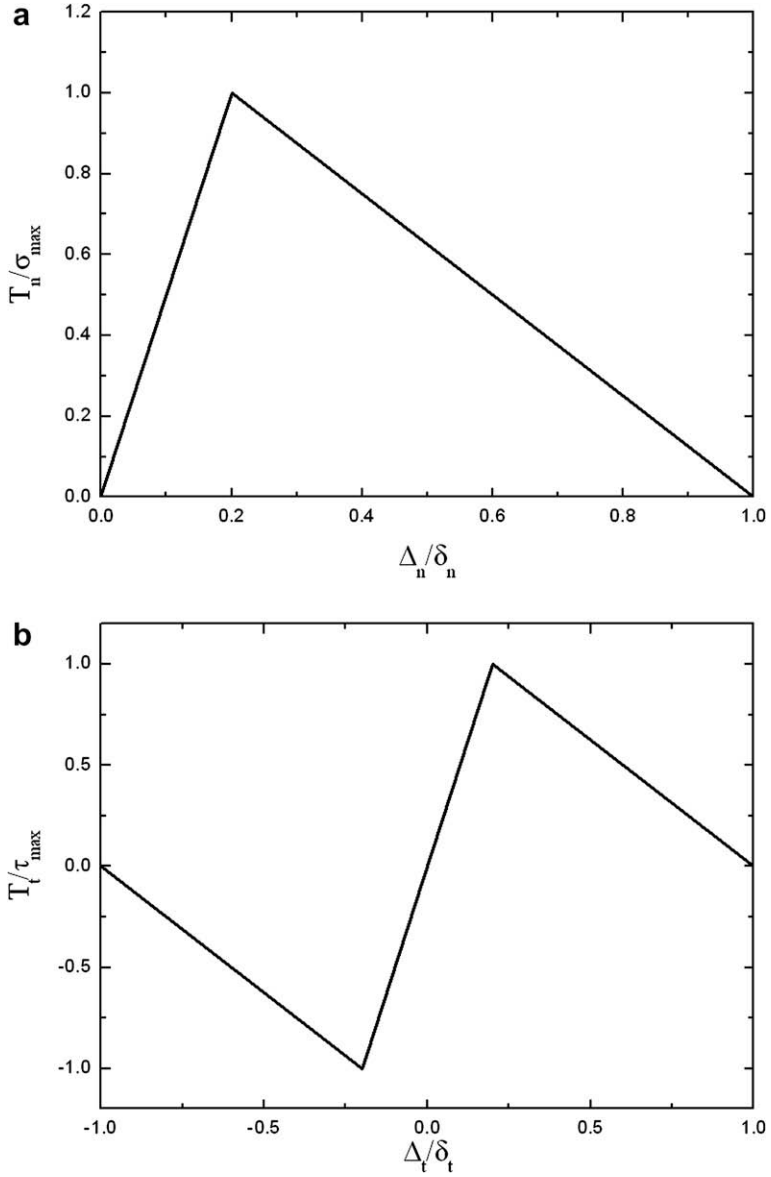

Fig. 4. (a) Normal and (b) tangential traction–separation curves for the bilinear CZM.

For pure opening ($\Delta_t = 0$) and pure shear separation ($\Delta_n = 0$), the normal and tangential tractions versus separations are graphically depicted in Fig. 4(a) and (b), respectively. The normal and tangential works of interface separation are given by

$$\phi_n = \sigma_{max}\Delta_n^c/2, \qquad \phi_t = \tau_{max}\Delta_t^c/2 \tag{10}$$

2.3. Trapezoidal CZM

The traction–separation relation used in the trapezoidal CZM is shown graphically in Fig. 5. A single non-dimensional separation parameter is defined as

$$\delta = \sqrt{\left(\delta_n/\delta_n^c\right)^2 + \left(\delta_t/\delta_t^c\right)^2} \tag{11}$$

such that the tractions drop to zero when $\delta = 1$. δ_n^c and δ_t^c in Eq. (11) are the critical values of these displacement components. By defining a potential as

$$\Phi(\Delta_n, \Delta_t) = \Delta_n^c \int_0^\delta \sigma(\delta')\, d\delta', \tag{12}$$

the normal and tangential tractions across the interface are given below as

$$T_n = \frac{\partial \Phi}{\partial \Delta_n} = \frac{\sigma(\delta)}{\delta}\delta_n, \qquad T_t = \frac{\partial \Phi}{\partial \Delta_t} = \frac{\sigma(\delta)}{\delta}\frac{\Delta_n^c}{\Delta_t^c}\delta_t. \tag{13}$$

The peak normal traction for pure normal separation is σ_{max}, while the peak tangential traction in pure tangential separation is $\tau_{max} = (\delta_n^c/\delta_t^c)\sigma_{max}$. The work of separation per unit area of interface Γ_0 is given by Eq. (12) with $\delta = 1$. For the separation function $\sigma(\delta)$, as specified in Fig. 5, we have

$$\Gamma_0 = \frac{1}{2}\sigma_{max}\Delta_n^c(1 - \delta_1 + \delta_2) \tag{14}$$

Regardless of the combination of normal and tangential displacements, the above work of separation is taking place in the cohesive zone, thus this trapezoidal CZM is mode-independent. In this CZM, the governing parameters of the cohesive law are the work of fracture, Γ_0; the peak stress, σ_{max}; and the critical displacement ratio, δ_n^c/δ_t^c, together with shape factors δ_1 and δ_2; however, some research has suggested that the details of the shape of the separation law are relatively unimportant, and the two most important parameters are Γ_0 and σ_{max} (e.g., Tvergaard and Hutchinson, 1992).

3. FEM model and simulation method

The numerical simulations of the interfacial delamination occurring in the above sandwiched cantilever tests were carried out with the aid of the finite element method (FEM) in the commercial code ABAQUS. The Cr/PZT interface is defined as a thin layer obeying the constitutive relation of a CZM. Accordingly, the elements along the interface are defined as cohesive elements. The corresponding constitutive relation of a CZM, i.e., the traction–separation relation of cohesive law, is implemented through the user subroutine UEL of ABAQUS. Other parts of the model keep their own material properties. Based on the geometric shape of the specimens and loading conditions, the plane strain state is assumed for the corresponding problems in order to simplify the simulations. In the numerical model, the regions near the free edge of interface were carefully divided into fine meshes, with a smallest element size of approximately 150 nm. The typical finite element mesh of the D2 specimen used in the simulations is shown in Fig. 6, which includes 2060 cohesive elements and 4120 nodes, plus 48,281 plane strain elements and 45,991 nodes.

Recalling the above constitutive relations of the three types of CZMs, the numerical simulations involved are non-linear in nature. Therefore, one critical issue is how to ensure the convergence of the calculation process. According to Gao and Bower (2004), when applying cohesive elements in a simulation, an elastic snap-back instability arising from crack initiation induces the solution to

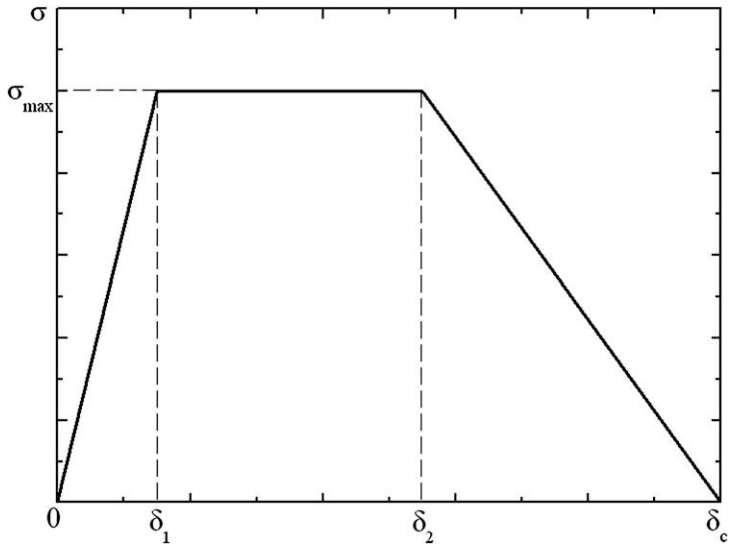

Fig. 5. Traction–separation relation used in the trapezoidal CZM.

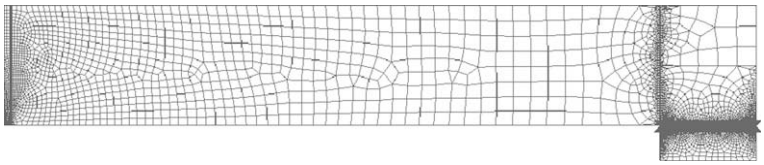

Fig. 6. Typical finite element mesh of the D2 sandwiched cantilever specimen.

quickly diverge from the equilibrium path. In order to overcome this difficulty, some modification is made to the CZM.

First, a small additional viscous dissipation, ζ (Gao and Bower, 2004) is introduced to the CZM. Taking the exponential CZM as an example, this technique is illustrated below. After the small viscous dissipation is introduced to the model, the constitutive relations become

$$T_n = \sigma_{max}\exp\left(1-\frac{\Delta_n}{\delta_n}\right)\left\{\frac{\Delta_n}{\delta_n}\exp\left(-\frac{\Delta_t^2}{\delta_t^2}\right) + \frac{1-q}{r-1}\left[\exp\left(-\frac{\Delta_t^2}{\delta_t^2}\right)\right]\left(r-\frac{\Delta_n}{\delta_n}\right)\right\} + \zeta_n\frac{d}{dt}\left(\frac{\Delta_n}{\delta_n}\right) \quad (15)$$

$$T_t = 2\sigma_{max}\left(\frac{\delta_n}{\delta_t}\right)\frac{\Delta_t}{\delta_t}\left(q+\frac{r-q}{r-1}\frac{\Delta_n}{\delta_n}\right)\exp\left(1-\frac{\Delta_n}{\delta_n}\right)\exp\left(-\frac{\Delta_t^2}{\delta_t^2}\right) + \zeta_t\frac{d}{dt}\left(\frac{\Delta_t}{\delta_t}\right) \quad (16)$$

where ζ_n and ζ_t are viscosity-like parameters governing the viscous energy dissipation under normal and tangential loadings, respectively. The intention of introducing the viscosity is not to model any physical energy dissipation process, but to regularize the instability when crack initiation occurs. Studies (Gao and Bower, 2004) have already shown that this method is very effective for cohesive zone modeling. In this work, all of the bilinear, trapezoidal, and exponential CZMs utilize this viscosity technique. Second, the region near the interface is carefully divided into fine meshes and the meshes take regular geometrical shapes. In addition to these, the incremental steps in the analysis are set small enough in order to ensure the convergence of the simulation process.

4. Results and discussion

4.1. Exponential CZM

The key parameters of the CZM include cohesive strength, work of separation, and the interface characteristic length parameter. A number of sets of these parameters are utilized in the simulation to best match the experimental results. Preliminary calculations reveal that the numerical results are less sensitive to the interface characteristic length parameter, δ_n, compared to the cohesive strength. For this reason, δ_n is set to 0.0015 μm in all of the simulations using the exponential CZM, and this choice of δ_n is able to ensure the convergence of the simulations as well. In contrast to δ_n, the cohesive strength has a prominent influence on the simulation results, as can be seen in Figs. 7 and 8 below.

Based on preliminary calculations, a reasonable value for the cohesive strength, σ_{max}, is found to be around 20–30 MPa. In order to better describe the simulation results, three values of σ_{max} are selected, including 24 MPa, 26 MPa, and 28 MPa. From the relation $q = \phi_t/\phi_n$ and Eq. (5), the corresponding values of the tangential cohesive strength, τ_{max}, are 27.98 MPa, 30.31 MPa, and 32.64 MPa, respectively. Note that the area under the traction–separation curve gives the work of separation. Therefore, the works of the normal separation related to the above σ_{max} are 0.0979 J/m^2, 0.1131 J/m^2, and 0.1142 J/m^2, respectively. Furthermore, the associated values of work of tangential separation are 0.04895 J/m^2, 0.05655 J/m^2, and 0.0571 J/m^2 accordingly.

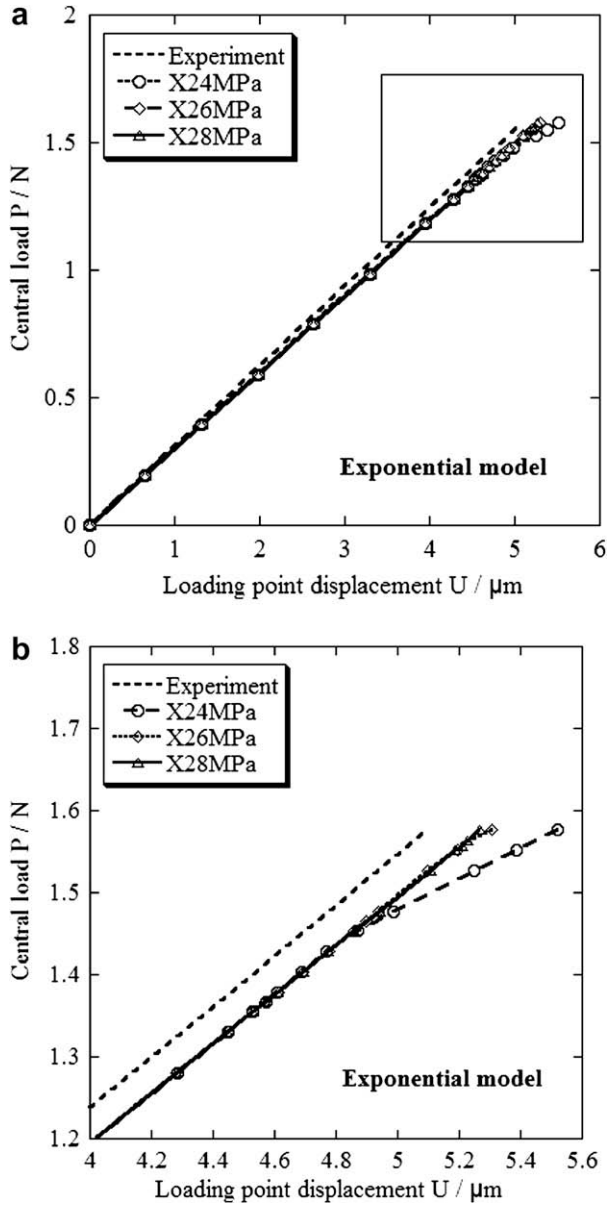

Fig. 7. Load–displacement curves with different cohesive strengths for the exponential CZM.

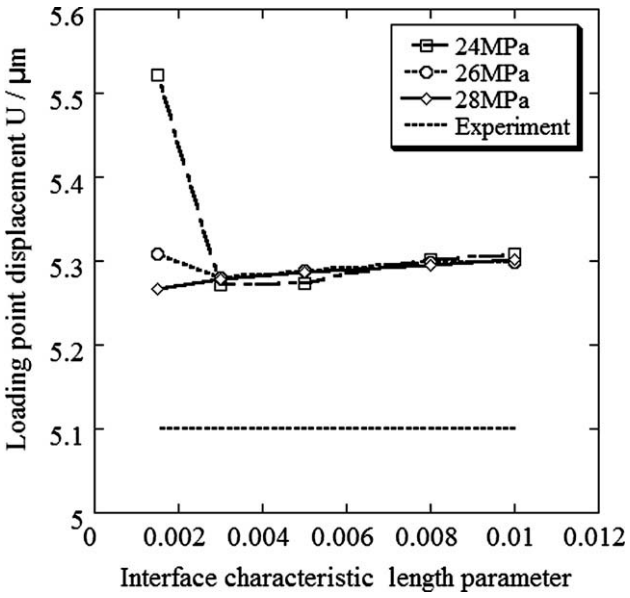

Fig. 8. Loading point displacements with different interface characteristic length parameters for the exponential CZM (under a fracture load of 1.576 N).

Table 1
Cohesive zone parameters, comparisons between the calculated and experimental results.

Parameter set		1	2	3	4	5
Interfacial length parameter (μm)			0.0015	0.0015		0.0015
Normal cohesive strength (MPa)		22	24	26	25	28
Work of normal separation (J/m^2)	Bilinear		0.12	0.13		0.14
	Exponential		0.0979	0.1131		0.1142
	Trapezoidal	0.132	0.144		0.15	
Work of tangential separation (J/m^2)	Bilinear		0.24	0.26		0.28
	Exponential		0.04895	0.05655		0.0571
	Trapezoidal	0.264	0.288		0.3	
Displacement at loading point (μm)	Bilinear		6.4316	5.8275		5.2531
	Exponential		5.5221	5.3079		5.2671
	Trapezoidal	6.1364	5.347		5.2541	
Measured displacement at loading point for D2 specimen (μm)		5.10				

Fig. 7 compares the load–displacement curves at the loading point obtained from the simulations and experiment. The right figure is an enlarged view of the square region of the left figure, which shows the details of the curves near the final fracture. The symbols in Fig. 7, for example "X24MPa," signify that the load–displacement curve is obtained with the exponential CZM at σ_{max} = 24 MPa, and so on. It is seen that, as the cohesive strength increases, the calculated curves become closer to the experimental curve. For the two cases of cohesive strength, σ_{max} = 24 and 26 MPa, and the calculated curves are close to the experimental curve except when approaching the final fracture point. For the σ_{max} = 28 MPa case, the calculated curve remains nearly straight during the entire loading process until the interface completely fractures, and is also very close to the experimental curve. Table 1 lists the calculated values of the displacements at the loading points for the three cases, together with the corresponding experimental data. From Table 1 and Fig. 7, it is seen that σ_{max} = 28 MPa provides more accurate predictions of the displacements at loading point than the other cohesive strengths. Numerical simulations also reveal that, if σ_{max} exceeds 28 MPa, interface cracking will not initiate, even though the calculated curve would approach the experimental curve.

Fig. 8 shows the influence of interface characteristic length parameters on the simulation results. For the cases of σ_{max} = 24 and 26 MPa, the displacement at the loading point initially increases and then decreases when δ_n is relatively small, but as δ_n exceeds 0.003 μm, the displacement keeps increasing with increasing δ_n. For the σ_{max} = 28 MPa case, the displacement at the loading point always keeps increasing with increasing δ_n. Because the increase in δ_n implies that the interface becomes soft, its stiffness should decrease. Therefore, the displacement at the loading point should become larger. With this in mind, setting σ_{max} to 28 MPa is more reasonable.

4.2. Bilinear CZM

The simulation results obtained from the bilinear CZM indicate that the displacement at the loading point is not sensitive to the interface characteristic length parameter δ_{max}. This observation is similar to that of the exponential CZM, the only difference being that in using the bilinear CZM the numerical convergence is quite sensitive to δ_{max}. When δ_{max} > 0.03 μm, the simulation converges extremely slowly. In order to solve this convergence problem and also to facilitate comparison with the exponential CZM, δ_{max} is set to 0.0015 μm in the bilinear CZM simulations. The normal cohesive strengths, σ_{max}, are given the values of 24 MPa, 26 MPa, and 28 MPa, and the corresponding tangential cohesive strengths, τ_{max}, are also given the same values of 24 MPa, 26 MPa, and 28 MPa, respectively. From Eq. (10), the works of normal separation are determined to be 0.12 J/m^2, 0.13 J/m^2, and 0.14 J/m^2, and the corresponding works of tangential separation are 0.24 J/m^2, 0.26 J/m^2, and 0.28 J/m^2, respectively.

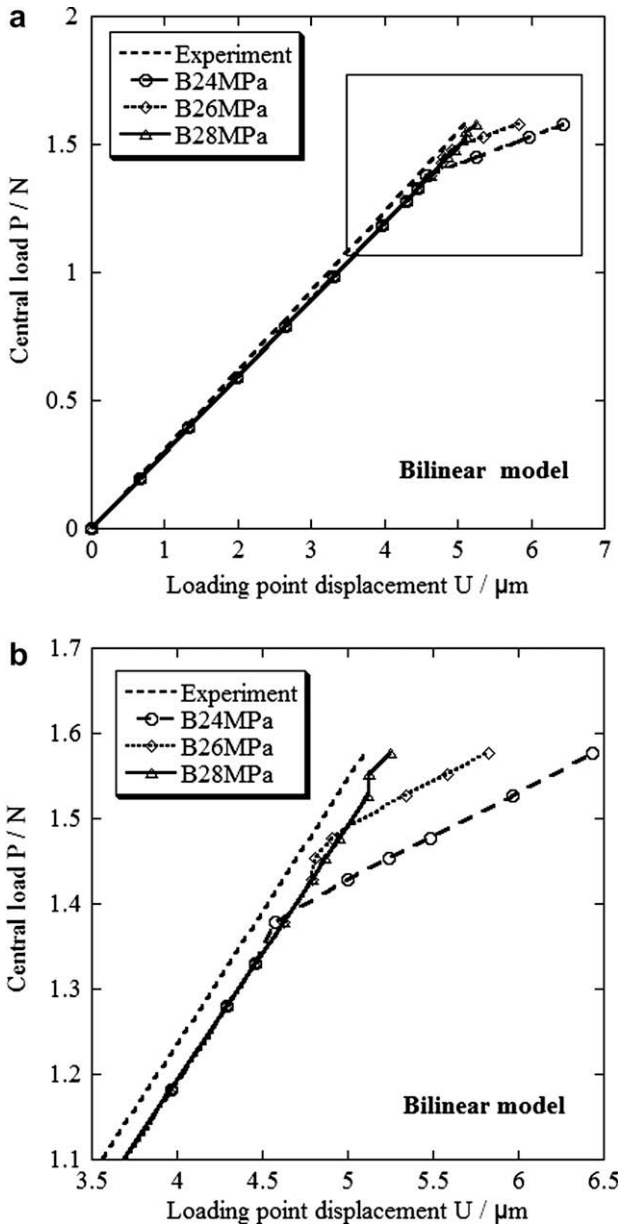

Fig. 9. Load–displacement curves for the bilinear CZM.

Fig. 9 shows the calculated results of the load–displacement curves at the loading point, together with the experimental curve. The symbols in Fig. 9, for example "B24MPa," signify that the load–displacement curve is obtained with the Bilinear CZM setting σ_{max} = 24 MPa, and so on. Again, as the cohesive strength increases, the calculated curves approach the experimental curve. For the two cases of σ_{max} = 24 and 26 MPa, most segments of the calculated curves are already close to the experimental curve; only when near the fracture load does the curves depart from it, representing the propagation process along the interface, which is observable from the deformation contour plot of the specimens during the simulations. For the σ_{max} = 28 MPa case, the calculated curve remains nearly straight during the entire loading process until the interface completely fractures, and the entire curve is largely consistent with the experimental curve. From Table 1 and Fig. 9, it is again seen that σ_{max} = 28 MPa provides more accurate predictions of the displacements at loading point when using the bilinear CZM. Furthermore, no cracking can propagate from the free edge of the interface when σ_{max} is set to be larger than 28 MPa, under the condition of a fracture load of 1.576 N.

4.3. Trapezoidal CZM

Similar to the above two cases, the interface characteristic length parameter δ_{max} also has less importance in the trapezoidal CZM. In the following simulations, δ_1 and δ_2 are set to 0.002 μm and 0.0025 μm, respectively. Preliminary calculations show that the normal cohesive strength, σ_{max}, is a bit lower than that in either exponential or bilinear CZM. Three values of σ_{max}, including 22 MPa, 24 MPa, and 25 MPa, are selected for illustrative purposes, and the corresponding tangential cohesive strengths, τ_{max}, are 11 MPa, 12 MPa, and 12.5 MPa, respectively. From Eq. (14), the corresponding values for the work of separation are 0.1155 J/m^2, 0.126 J/m^2, and 0.13125 J/m^2, respectively.

Fig. 10 depicts the calculated results of the load–displacement curves at the loading point and compares them with the experimental curve. The symbols in Fig. 10, for example "T22MPa," signify that the load–displacement curve is obtained with the trapezoidal CZM setting of σ_{max} = 22 MPa, and so on. The figures indicate that the calculated curves approach the experimental curve as the cohesive strength increases. Putting σ_{max} = 25 MPa, the calculated curve remains nearly straight during the entire loading process until the interface completely fractures, and the entire curve becomes more consistent with the experimental curve. Furthermore, no cracking can propagate along the interface when σ_{max} is set to be larger than 25 MPa, under the condition of a fracture load of 1.576 N.

4.4. Comparisons of the simulation results obtained from cohesive zone modeling

Fig. 11 collects the results of the load–displacement curves obtained from all of the above CZM simulations. For the three types of CZMs, the same tendency appears in that the calculated curves better match the experimental curve when increasing the cohesive strength. For the exponential and bilinear CZMs, setting the cohesive strength to 28 MPa gives the best predictions. For the trapezoidal CZM, the proper choice is σ_{max} = 25 MPa. It is seen that the calculated curves from the bilinear CZM agree comparatively well with the experimental curve for the entire cracking process, from initiation to propagation along the interface. Furthermore, it is seen from Table 1 that the error of the calculated displacements at the loading point relative to the experimental value are smallest from the bilinear CZM among the three CZMs. Based on the above points, the bilinear CZM is arguably more suitable than the other two CZMs in characterizing this interfacial delamination.

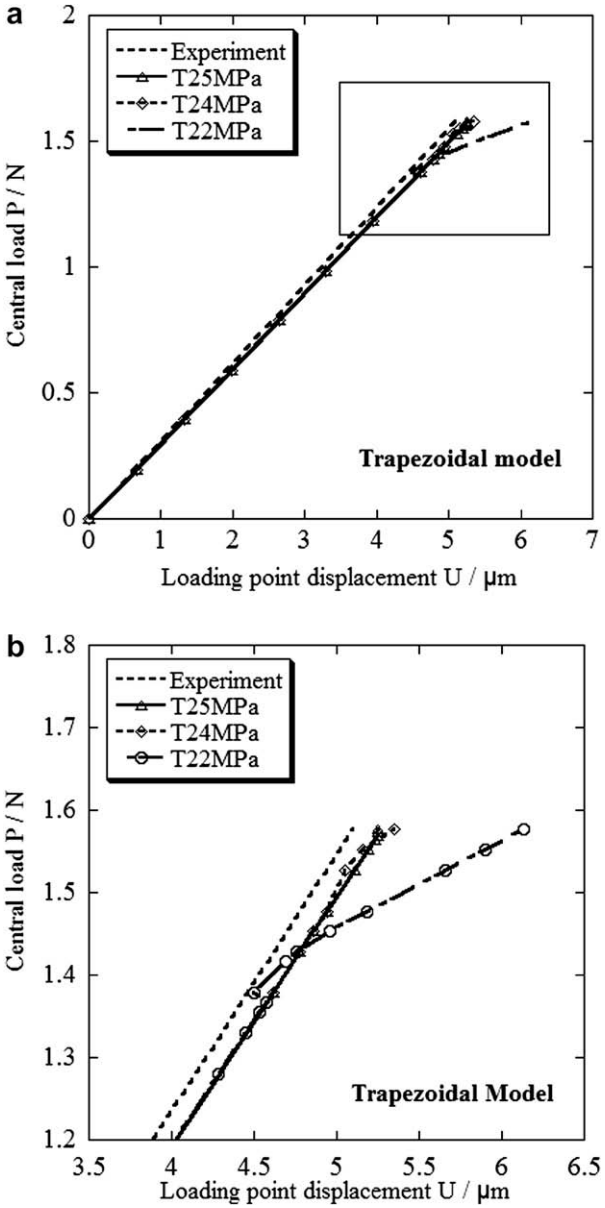

Fig. 10. Load–displacement curves for the trapezoidal CZM.

Fig. 12(a) shows the distributions of the normal tractions along the entire Cr/PZT interface for the three CZMs at the moment of crack initiation, where the abscissa is the relative distance along the interface normalized by the length of the interface. It is seen that, with increasing cohesive strength, the length of the interface region that is already fractured becomes shorter, and the crack length from the bilinear CZM is the longest among the three CZMs for the same cohesive strength. Moreover, the normal tractions along the fractured region for the bilinear CZM are nearly zero, while that for the trapezoidal and exponential CZMs are not. Judging from these points, the bilinear CZM is again more appropriate in describing this interfacial delamination. Recalling the experimental evidence of this delamination process observed in the sandwiched cantilever tests, we argue that the bilinear CZM is more suitable in modeling the brittle fracture process. It is worth mentioning here one recent study by Yamakov et al. (2006), in which molecular dynamics simulations of intergranular fracture processes in aluminum were developed. Their work justified the use of a trapezoidal type of CZM law for elasto-plastic fracture

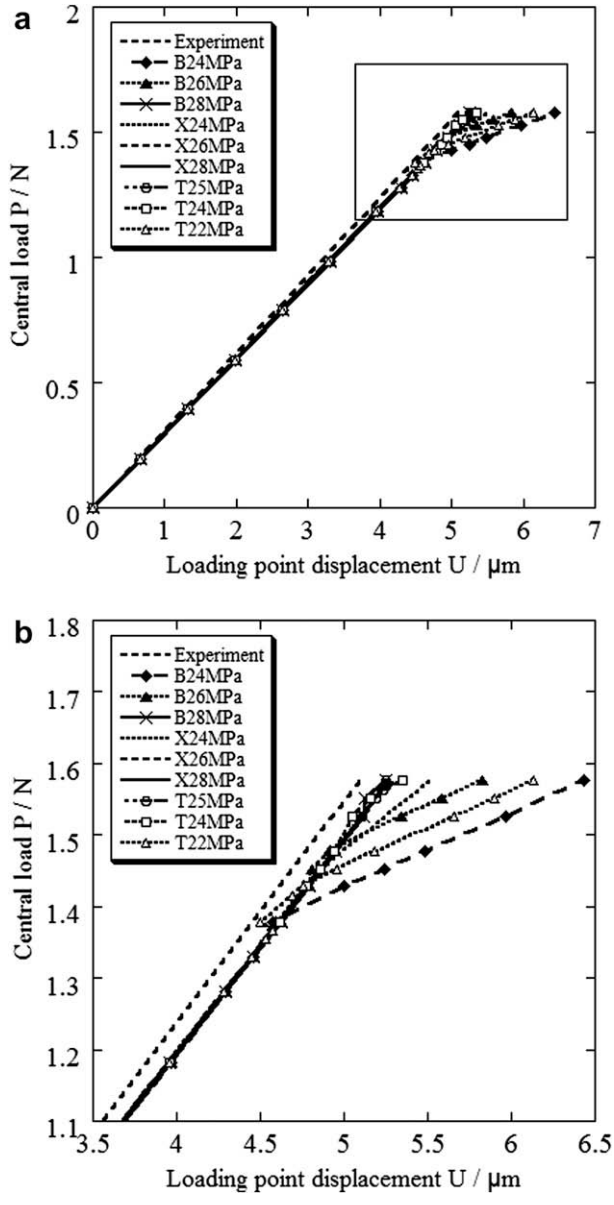

Fig. 11. Comparisons of the load–displacement curves from the three CZMs to the experimental curve.

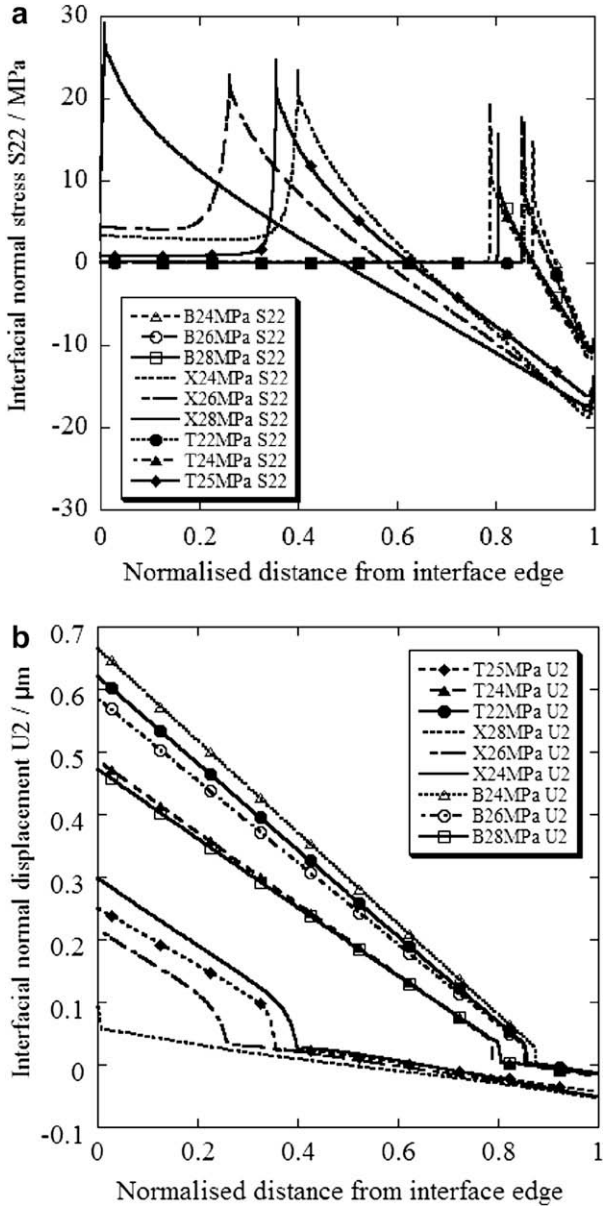

Fig. 12. Distributions of the normal tractions and the displacements along the Cr/PZT interface.

and a bilinear CZM law for brittle fracture, a result which agrees with the conclusions of our study.

Fig. 12(b) shows the distributions of the normal displacements (interfacial separation) along the Cr/PZT interface for the three CZMs when cracks start. Because the sandwiched-cantilever specimens are subjected to bending conditions during tests, the normal component of the interface displacement is dominant. It is seen that, by increasing the cohesive strength for a given CZM, the interfacial normal displacement decreases and the crack length shortens as well. For the exponential CZM, the crack length is minute at $\sigma_{max} = 28$ MPa, whereas as σ_{max} reaches 24 MPa, nearly 40% of the entire interface region has already fractured. In contrast with the exponential CZM, more that 80% of the interface region in the bilinear CZM has fractured for all values of the cohesive strengths. These comparisons validate again the reasoning behind adopting the bilinear CZM.

Table 1 summarizes the calculated displacements at the loading point for all three CZM simulations, together with the measured displacements. It is apparent that the bilinear CZM coupled with the 5th set of parameters produce the best predictions, with a relative error of about 3%, when compared to those from experiment.

Based on the above results, it can be concluded that the bilinear CZM is more appropriate in studying delamination along the Cr/PZT interface in these piezoelectric thin films. The corresponding CZM parameters for the Cr/PZT interface have thus been extracted, specifically, the interface characteristic length, $\delta_{max} = 0.0015$ μm; cohesive strength, $\sigma_{max} = 28$ MPa; work of normal separation, $\phi_n = 0.14$ J/m^2; and work of tangential separation, $\phi_t = 0.28$ J/m^2.

4.5. Verification of CZM parameters

All of the above simulations were carried out for the D2 specimen, and therefore, the derived CZM parameters reflect only the influence of geometry and loading conditions of the D2 specimen. Other tested specimens, such as the D1 and D3 specimens, are made of the same material and their fracture features are

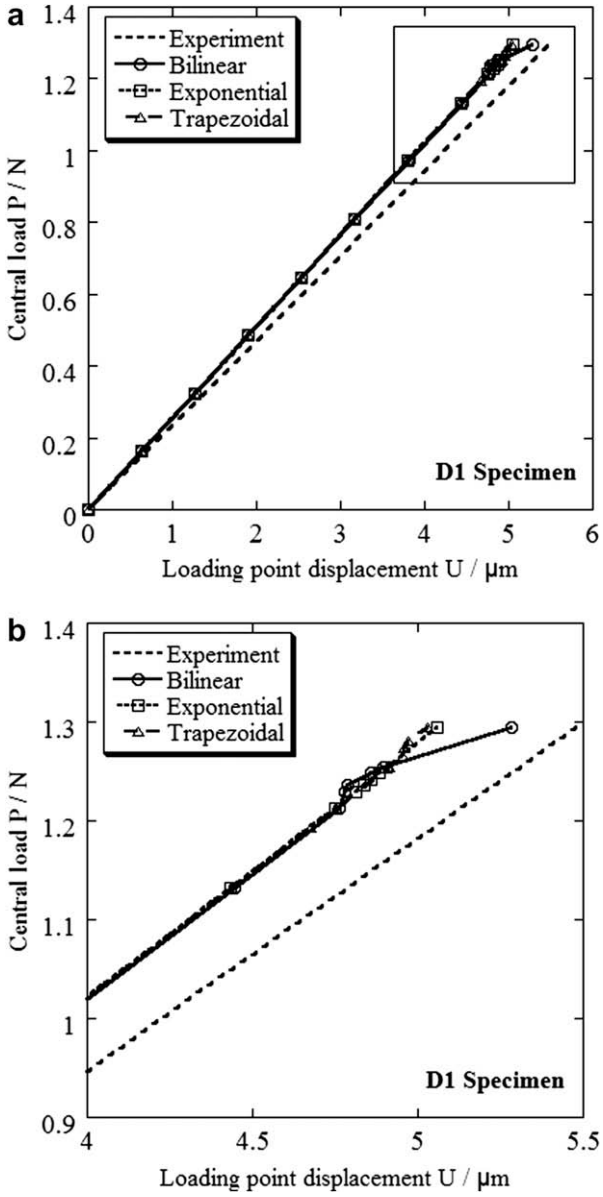

Fig. 13. Comparison of the calculated curves to the experimental curve of specimen D1.

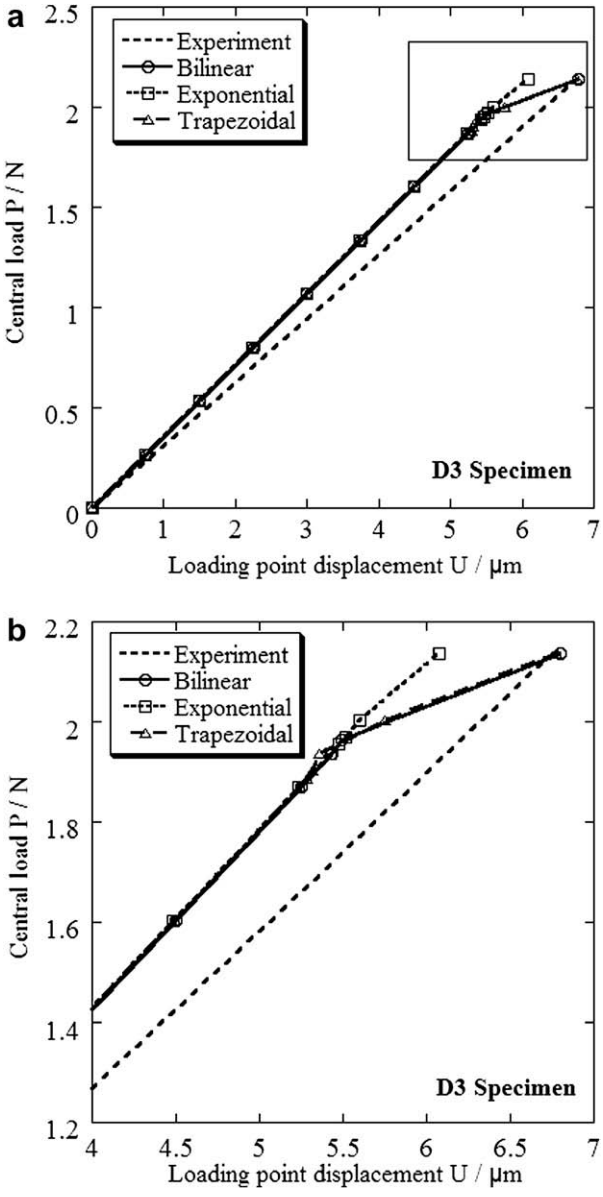

Fig. 14. Comparison of the calculated curves to the experimental curve of specimen D3.

also identical to those of the D2 specimen. Therefore, the CZM parameters obtained in our study can be easily verified by applying the same CZM parameters in the simulations of the D1 and D3 specimens, and then by verifying against experimental results. The results are displayed in Figs. 13 and 14, wherein the 5th set of parameters in Table 1 is used for both bilinear and exponential CZMs and the 4th set of parameters for the trapezoidal CZM.

In Figs. 13 and 14, the tendencies of all of the calculated curves for the D1 and D3 specimens are consistent with the experimental curve. Near the final fracture point, the calculated curves from the bilinear CZM best match the experimental curve. The relative errors of the calculated displacement at the loading point are relatively small, as also shown in Table 2. The prediction value errors from the bilinear CZM are less than 4%, while those from the exponential CZM are relatively higher, thus verifying that these CZM parameters are reliable and can be used to predict the delamination process along the Cr/PZT interface of the piezoelectric thin films.

4.6. Bonding strength of the Cr/PZT interface

The cohesive strength and the work of separation for the Cr/PZT interface in the multilayered thin films are discussed in this section.

From the above simulations, the values of the characteristic parameters of the Cr/PZT interface are determined to be as follows: cohesive strength, $\sigma_{max} = 28$ MPa; work of normal separation, $\phi_n = 0.14\ J/m^2$; and work of tangential separation, $\phi_t = 0.28\ J/m^2$. It is well known that the rupture strength of bulk Cr material is about 80 MPa, and the bending strengths of typical ceramics are around several hundreds of MPa. By comparing the cohesive strength of 28 MPa of the Cr/PZT interface with these values, it can be stated that this interface is not strongly bonded. According to Freund and Suresh (2003), the interface fracture toughness of thin films or coatings of millimeter thickness can be as low as $0.5\ J/m^2$ and higher than $300\ J/m^2$, and typically weak interfaces have low fracture energies in the range of 1–10 J/m^2. After a comprehensive review of some results of interfacial toughness mea-

Table 2
Comparisons of the calculated results for the specimens D1 and D3 with their experimental results.

Specimen No.		D1	D3
Fracture load (N)		1.294	2.136
Calculated displacement at loading point (μm)	bilinear	5.2825	6.7964
	Exponential	5.0575	6.0791
	Trapezoidal	5.0287	6.7729
Measured displacement at loading point (μm)		5.48	6.76
Relative error (%)	Bilinear	3.60	0.54
	Exponential	7.71	10.07
	Trapezoidal	8.24	0.19

surements for about 25 film/substrate multilayered systems, Volinsky et al. (2002) showed that film systems, such as those with carbon as a contaminant between Al, Al_2O_3, or SiO_2 film layers, can have a very low adhesion toughness, e.g., 0.25–0.33 J/m^2. They also observed that, when increasing the film thickness from 200 to 2000 nm, there is a remarkable increase in fracture resistance from about 4 to 12 J/m^2 for strong interfaces like Al/innerlayer/SiO_2 or Al/innerlayer/Al_2O_3, as long as the inner layer is reasonably thin. From our results (0.14 J/m^2, 0.28 J/m^2), we remark that the Cr/PZT interface in the Cr/PZT/PLT/Pt/Ti/Si film system investigated in this work has a relatively low bonding strength, and is a weak interface. In this multilayered thin film, the Cr layer is only 0.2 μm thick while the PZT layer is about 2.5 μm thick. The other three film layers are all thinner than the PZT layer, e.g., the PLT and Ti layers are about 20 nm thick. Therefore, it might be reasonable that the Cr/PZT interface here does have such a low fracture energy.

5. Conclusions

In this work, three types of cohesive zone models, together with finite element methods, were employed to simulate the fracture process along the Cr/PZT interface in thin films. The simulation results reveal that, for the exponential, trapezoidal, and bilinear CZMs, cohesive strength and work of separation are the dominant parameters, and the interface characteristic length parameter is less important. Through calibration with the experimental results, the bilinear CZM was found to be more suitable than the other two CZMs in describing Cr/PZT interfacial delamination. The characteristic values of its cohesive strength and work of separation were found to be 28 MPa and 0.14 J/m^2, respectively. These results show that the critical interfacial stress for crack initiation is apparently lower than the rupture strength of bulk PZT or Cr. By comparing the fracture energies of typical films or coating materials of several millimeter thicknesses, the fracture energy of this Cr/PZT interface is also quite low. It is thus confirmed that the examined Cr/PZT interface is weakly bonded and its fracture process is characterized as brittle. Our study demonstrated the applicability of the cohesive zone model in characterizing the interface fracture behavior of micro-thick film materials.

Acknowledgments

This work was financially supported by the National Natural Science Foundation of China through Grant No. 90607013. The authors gratefully thank the two anonymous reviewers for helpful comments.

References

Akisanya, A.R., Meng, C.S., 2003. Initiation of fracture at the interface corner of bi-material joints. Journal of the Mechanics and Physics of Solids 51 (1), 27–46.
Barenblatt, G.I., 1962. Mathematical theory of equilibrium cracks in brittle fracture. Advances in Applied Mechanics 7, 55–125.
Becker Jr., T.L., McNancy, J.M., Cannon, R.M., Ritchie, R.O., 1997. Limitations on the use of the mixed mode delamination beam test specimen: effect of the size of the region of K-dominance. Materials of Mechanics 25 (4), 291–308.
Camacho, G.T., Ortiz, M., 1996. Computational modeling of impact damage in brittle materials. International Journal of Solids and Structures 33 (20-22), 2899–2938.
Chandra, N., Li, H., Shet, C., Ghonem, H., 2002. Some issues in the application of cohesive zone models for metal–ceramic interfaces. International Journal of Solids and Structures 39 (10), 2827–2855.
Dugdale, D.S., 1960. Yielding of steel sheets containing slits. Journal of the Mechanics and Physics of Solids 8 (2), 100–104.
Evans, A.G., Hutchinson, J.W., 1995. The thermo-mechanical integrity of thin films and multilayers. Acta Metallurgical Materials 43 (7), 2507–2530.
Feraren, P., Jensen, H.M., 2004. Cohesive zone modelling of interface fracture near flaws in adhesive joints. Engineering Fracture Mechanics 71 (15), 2125–2142.
Freund, L.B., Suresh, S., 2003. Thin Film Materials. Cambridge University Press, Cambridge.
Gao, Y.F., Bower, A.F., 2004. A simple technique for avoiding convergence problems in finite element simulation of crack nucleation and growth on cohesive interfaces. Modelling and Simulation in Materials Science and Engineering 12 (3), 453–463.
Geubelle, P.H., Baylor, J., 1998. Impact-induced delamination of laminated composites: a 2D simulation. Composites Part B: Engineering 29 (5), 589–602.
Kong, X.D., En, Y.F., 2006. Failure Analysis and Cases of Electronic Components. Defense Industrials Press, Beijing.
Mohammed, I., Liechti, K.M., 2000. Cohesive zone modeling of crack initiation at biomaterial corners. Journal of the Mechanics and Physics of Solids 48 (4), 735–764.
Needleman, A., 1987. A continuum model for void nucleation by inclusion debonding. Journal of Applied Mechanics 54, 525–531.
Needleman, A., 1990. An analysis of tensile decohesion along an interface. Journal of the Mechanics and Physics of Solids 38 (3), 289–324.
Shang, F., Kitamura, T., Hirakata, H., Kanno, I., Kotera, H., Terada, K., 2005. Experimental and theoretical investigations of delamination at free edge of interface between piezoelectric thin films on a substrate. Int. J. Solids Struct. 42 (5–6), 1729–1741.
Tvergaard, V., Hutchinson, J.W., 1992. The relation between crack growth resistance and fracture process parameters in elastic–plastic solids. Journal of the Mechanics and Physics of Solids 40 (6), 1377–1397.
Volinsky, A.A., Moody, N.R., Gerberich, W.W., 2002. Interfacial toughness measurements for thin films on substrates. Acta Materialia 50 (3), 441–466.
Wei, Y.G., Hutchinson, J.W., 1997. Nonlinear delamination mechanics of thin films. Journal of the Mechanics and Physics of Solids 45 (7), 1137–1159.
Xu, X.P., Needleman, A., 1993. Void nucleation by inclusion debonding in a crystal matrix. Modelling and Simulation in Materials Science and Engineering 1 (2), 111–132.
Xu, X.P., Needleman, A., 1994. Numerical simulations of fast crack growth in brittle solids. Journal of the Mechanics and Physics of Solids 42 (9), 1397–1434.
Yamakov, V., Saether, E., Phillips, D.R., Glaessgen, E.H., 2006. Molecular-dynamics simulation-based cohesive zone representation of intergranular fracture processes in aluminum. Journal of the Mechanics and Physics of Solids 54 (9), 1899–1928.
Yang, B.Q., Chen, G.N., Zhang, K., Luo, G.X., Xiao, J.H., 2007. A review on measurement methods for interfacial bonding strength between coating and substrate. Chinese Journal of Advances in Mechanics 37 (1), 67–79.